Sq current system during stratospheric sudden warming events in 2006 and 2009

Yosuke Yamazaki,[1] Arthur D. Richmond,[1] Huixin Liu,[2,3] Kiyohumi Yumoto,[2,3] and Yoshimasa Tanaka[4]

Received 11 July 2012; revised 19 September 2012; accepted 22 October 2012; published 20 December 2012.

[1] Ionospheric Sq current systems during unusually strong and prolonged stratospheric sudden warming (SSW) events in January 2006 and January 2009 are examined by analyzing ground-magnetometer data for the American and Asian longitude sectors. During these SSW events, a significant decrease and increase of the Sq equivalent current intensity are observed in the Northern and Southern Hemispheres, respectively, along with a reduction in the longitudinal separation between the northern and southern current vortices. Numerical experiments using the National Center for Atmospheric Research Thermosphere-Ionosphere-Electrodynamics General-Circulation Model show that changes in the solar anti-symmetric (2,3) semidiurnal tide can bring about similar changes in the Sq current system.

Citation: Yamazaki, Y., A. D. Richmond, H. Liu, K. Yumoto, and Y. Tanaka (2012), Sq current system during stratospheric sudden warming events in 2006 and 2009, *J. Geophys. Res.*, *117*, A12313, doi:10.1029/2012JA018116.

1. Introduction

[2] In the dynamo region of the ionosphere (approximately 100–150 km altitude), atmospheric tides dominate the wind system. According to wind-dynamo theory [e.g., *Richmond*, 1979, 1989], these tides can generate electromotive forces and drive electric currents by moving the electrically conducting air in the ionosphere through the Earth's magnetic field. It has been demonstrated by model calculations that the ionospheric wind-dynamo currents can quantitatively explain the daily variation of the geomagnetic field at middle and low geomagnetic latitudes (below 60°) [e.g., *Richmond and Roble*, 1987]. During geomagnetically quiet periods, the daily variation of the geomagnetic field is mainly composed of solar 24-hour (30–60%), 12-hour (20–40%), 8-hour (10–20%), and 6-hour (>10%) tidal components, and is often referred to as the Sq (solar quiet-day) variation. The ionospheric current system responsible for the Sq variation is mainly driven by the solar diurnal tide that is locally generated by solar heating in the dynamo region of the ionosphere [*Takeda and Maeda*, 1980]. Additionally, upward-propagating tides (mainly solar semidiurnal tides) from the troposphere and stratosphere make some contribution in driving the ionospheric Sq current system [*Richmond and Roble*, 1987]. The analysis of the Sq variation, thus, can provide useful information about tidal changes in the upper atmosphere.

[3] Recent studies have shown that the ionosphere can be significantly disturbed during stratospheric sudden warming (SSW) events. The SSW is a meteorological phenomenon that can disrupt the typical wintertime circulation of the middle atmosphere [e.g., *Andrews et al.*, 1987]. During an SSW, the normal stratospheric polar vortex, characterized by eastward winds around a cold pole, breaks down. This process is triggered by abnormally enhanced planetary waves that propagate upward from the troposphere to the middle atmosphere. The breakdown of the stratospheric polar vortex reduces the southward Coriolis force that is in near-geostrophic balance with the northward pressure gradient force. Therefore, a poleward meridional wind is induced and downwelling in the polar stratosphere is increased, causing a rapid increase of the polar stratospheric temperature due to adiabatic heating. The main characteristics of the SSW in the middle atmosphere can be well reproduced by general circulation models (GCMs) [e.g., *Liu and Roble*, 2002; *Fuller-Rowell et al.*, 2010; *de la Torre et al.*, 2012].

[4] Observations during recent SSW events have shown significant changes in ionospheric parameters such as the equatorial electrojet [*Vineeth et al.*, 2009; *Sridharan et al.*, 2009; *Fejer et al.*, 2010; *Stening*, 2011; *Park et al.*, 2012], equatorial $\mathbf{E} \times \mathbf{B}$ vertical plasma drift [*Chau et al.*, 2009; *Anderson and Araujo-Pradere*, 2010; *Fejer et al.*, 2011], and total electron content (TEC) [*Chau et al.*, 2010; *Goncharenko et al.*, 2010a, 2010b; *Pedatella and Forbes*, 2010; *Yue et al.*, 2010; *Liu et al.*, 2011] (see also a review by *Chau et al.* [2011] and references therein). Most of the reported ionospheric variability indicates semidiurnal signatures characterized by an increase during local morning hours and decrease during local afternoon hours. Therefore,

[1]High Altitude Observatory, National Center for Atmospheric Research, Boulder, Colorado, USA.
[2]International Center for Space Weather Science and Education, Kyushu University, Fukuoka, Japan.
[3]Department of Earth and Planetary Sciences, Faculty of Sciences, Kyushu University, Fukuoka, Japan.
[4]National Institute of Polar Research, Tachikawa, Japan.

Corresponding author: Y. Yamazaki, High Altitude Observatory, National Center for Atmospheric Research, 3080 Center Green Dr., Boulder, Colorado, USA. (yamazaki@ucar.edu)

0148-0227/12/2012JA018116

it is believed that changes in the atmospheric semidiurnal tide play an important role in producing ionospheric variability during SSW events. As a matter of fact, mesospheric tidal observations have recorded significant changes during SSW events [*Wu et al.*, 2011; *Lima et al.*, 2012; *Sridharan et al.*, 2012].

[5] There are several mechanisms that may cause tidal changes during an SSW event. One possible mechanism is the modulation of upward propagation of the atmospheric tide due to changes in wind and temperature fields. *Stening et al.* [1997], using a numerical model, demonstrated that the distribution of background zonal winds in the middle atmosphere has a significant influence on amplitude and phase structures of the atmospheric tide. A numerical study by *McLandress* [2002] indicated that tidal amplitude and phase in the lower thermosphere are significantly affected by a latitudinal shear in zonal mean winds in the lower and middle atmosphere. Thus, one can expect that rapid and large changes in latitude and height structure of the zonal mean wind during an SSW event may lead to significant tidal changes in the lower thermosphere. Another possible mechanism for tidal changes during an SSW event is the interaction between planetary waves and tides. A simulation study by *Liu et al.* [2010] suggested that, although the planetary waves excited in the troposphere cannot propagate up to the ionosphere with significant amplitudes, the interaction between the planetary waves and tides can significantly modulate the tides, resulting in global ionospheric variability through ionospheric wind-dynamo processes. *Pedatella and Forbes* [2010] observed a correlation between planetary-wave activity in the stratosphere and tidal activity in the ionosphere during the January 2009 SSW event, supporting this idea. Another mechanism, suggested by *Goncharenko et al.* [2012], is tidal modulation due to changes in the stratospheric ozone density during SSW events. Solar-radiation absorption by stratospheric ozone is one of the main sources for upward-propagating solar semidiurnal tides.

[6] Some researchers have recognized that the amplification of the atmospheric lunar tide sometimes makes a significant contribution to the ionospheric variability during SSW events [*Fejer et al.*, 2010, 2011; *Park et al.*, 2012; *Yamazaki et al.*, 2012a, 2012b]. *Yamazaki et al.* [2012a] observed significant amplifications of the geomagnetic lunar tide at an equatorial station, Addis Ababa, in 70% of the major SSW events during the period 1958–2002. The amplification of the geomagnetic lunar tide indicates the amplification of the atmospheric lunar tide in the dynamo region of the ionosphere. *Pedatella et al.* [2012], using a numerical model, demonstrated that the inclusion of the lunar tidal forcing in the model is necessary to reproduce observed features of the equatorial $\mathbf{E} \times \mathbf{B}$ vertical plasma drift during SSW events.

[7] In contrast to increasing evidence for the importance of the lunar tide, the role of the atmospheric solar tide during SSW events is full of uncertainties. Simulation results by the TIMEGCM model indicate an increase in the solar diurnal and semidiurnal tides [*Liu et al.*, 2010]. (Note that their results were not for an actual SSW event but for an idealized planetary wave forcing, thus may not be entirely representative of the change during an SSW.) Simulation of the January-2009 SSW event by the Whole Atmosphere Model (WAM) indicates a decrease of the solar semidiurnal migrating tide and increase of the solar terdiurnal migrating tide in the middle atmosphere [*Fuller-Rowell et al.*, 2011; *Wang et al.*, 2011]. Mesospheric wind observations from TIMED satellite showed an increase of the semidiurnal tide at midlatitudes of the winter hemisphere during SSW events, but not always consistently [*Wu et al.*, 2011].

[8] One difficulty in the study of the SSW-ionosphere coupling arises from the fact that the upper atmospheric variability during SSW events is not always consistent, even though the SSW events are selected in a single uniform way. An SSW event is usually defined based on stratospheric parameters only (i.e., zonal mean zonal wind and temperature at 10 hPa), and middle and upper atmospheric processes are not considered. Thus, middle and upper atmospheric responses can be quite different from one SSW event to another. This is probably why some SSW events cause greater ionospheric variability than others. To avoid this complication, the present work focuses on a case study of two extreme events in January 2006 and January 2009. It has been reported that these SSW events are unusually strong and prolonged [*Manney et al.*, 2009]. The breakdown of the polar vortex during these events caused a polar wind reversal that extended from the lower stratosphere to the upper mesosphere [*Manney et al.*, 2008, 2009], and also caused subsequent anomalous stratopause structure in February and March [*France et al.*, 2012].

[9] In the present study, we analyze ground-magnetometer data during the SSW events in January 2006 and January 2009 to study effects of SSW on the ionospheric Sq current system. Our results suggest that, during these SSW events, the ionospheric Sq current system is significantly and consistently changed. Through the use of a general circulation model, results are interpreted in terms of changes in the atmospheric solar semidiurnal tide.

2. Data and Model

[10] We analyze one-minute-resolution geomagnetic field data to derive the ionospheric Sq current system. The ground magnetometer data are obtained mainly from the INTErnational Real-time MAGnetic Observatory NETwork (INTERMAGNET) [*Kerridge*, 2001; *Love*, 2008]. The stations used in this study are listed in Table 1, including both INTERMAGNET stations and other stations. In this paper, three orthogonal components of the geomagnetic field, H (geomagnetic northward), D (geomagnetic eastward), and Z (downward), are used.

[11] We use the National Center for Atmospheric Research Thermosphere-Ionosphere-Electrodynamics General-Circulation Model (NCAR/TIE-GCM) [*Richmond et al.*, 1992] for a mechanistic study in Section 3.3. The NCAR/TIE-GCM is a three-dimensional model of the coupled thermosphere and ionosphere. Although the model does not include the lower- and middle-atmosphere processes related to the SSW, a comparison between observations and model results with different tidal forcings at the lower boundary of the model is useful for the interpretation of the observations. The NCAR/TIE-GCM calculates ionospheric wind-dynamo processes, besides other physical and chemical processes, in the global thermosphere-ionosphere system between approximately 97 and 500 km altitudes. The horizontal

Table 1. Coordinates of Stations Used in the Study

Station	Code	GMLat.[a]	GMLon.[a]
	American Sector		
Ottawa	OTT	55.2°N	355.8°E
Fredericksburg	FRD	48.0°N	353.8°E
Bay St. Louis	BSL	39.7°N	340.3°E
Del Rio	DLR	38.0°N	327.8°E
San Juan	SJG	28.0°N	6.5°E
Kourou	KOU	14.6°N	20.0°E
Huancayo	HUA	1.9°S	356.9°E
Vassouras	VSS	13.4°S	27.2°E
Trelew	TRW	33.1°S	5.9°E
Port Stanley	PST	41.7°S	11.8°E
Argentine Island	AIA	55.1°S	5.8°E
	Asian Sector		
Irkutsk	IRT	41.2°N	177.2°E
Memambetsu	MMB	35.4°N	211.7°E
Kakioka	KAK	27.4°N	209.1°E
Okinawa[b]	OKN	17.0°N	198.9°E
Ponape[b]	PON	0.5°N	230.0°E
Kakudu	KDU	22.0°S	205.9°E
Alice Springs	ASP	32.6°S	208.5°E
Canberra	CNB	42.3°S	227.1°E
Eyrewell	EYR	46.8°S	253.9°E

[a]GMLat. and GMLon. denote dipole-geomagnetic latitude and longitude, respectively. †The data at the OKN station are provided by Geospatial Information Authority of Japan (GSI) Geomagnetic Survey.

[b]The data at the PON station are provided by the Ocean Hemisphere Project Data Management Center (OHP DMC).

resolution of the model is 5° × 5° in geographic longitude and latitude, and there are two grid points per scale height in the said height range. For a given day of year (*DoY*), magnetic activity index *Kp*, and solar activity index *F*10.7, electric currents are calculated in magnetic apex coordinates [*Richmond*, 1995] using a realistic magnetic field model (International Geomagnetic Reference Field, or IGRF). Geomagnetic daily variations at the ground are calculated from height-integrated horizontal currents as described by *Doumbia et al.* [2007] and A. D. Richmond and A. Maute (Ionospheric electrodynamics modeling, submitted to *Geophysical Monograph Series* of AGU, 2012). It is known that the NCAR/TIE-GCM underestimates E-region electric densities. To obtain realistic E-region ionospheric densities, an adjustment is made in the soft X-ray fluxes (between 8 and 70 Å) as described by *Fang et al.* [2008].

3. Results and Discussion

3.1. SSW Events

[12] Figure 1a shows a height-time section of the polar cap temperature (northward of 70° latitude) for the winter months of 2005–2006, as observed by Microwave Limb Sounder (MLS) instrument on NASA's Aura satellite. Plotted in Figure 1b are the zonal mean zonal wind at 60°N at 10 hPa (blue line) and the corresponding climatological seasonal cycle (red line), obtained from the National Centers for Environmental Prediction-National Center for Atmospheric Research (NCEP-NCAR) reanalysis [*Kalnay et al.*, 1996]. The pressure level 10 hPa is a representative altitude of the stratosphere (approximately 32 km height). A reversal of the zonal mean wind from eastward to westward indicates the occurrence of a major SSW event (the conditions for a major SSW event were fulfilled on January 21). After the peak reversal of the zonal wind on January 26, the polar stratopause became ill defined and then reformed at a considerably high altitude (>75 km). An SSW event that accompanies an abnormally high stratopause is classified as an elevated stratopause event [e.g., *Chandran et al.*, 2011]. As can be seen in Figure 1a, it takes more than one month until the height of the stratopause goes back to the normal level (45–55 km).

[13] Figures 1c and 1d depict daily variations of the geomagnetic field ΔH at Fredericksburg (FRD) and Port Stanley (PST), respectively. The Δ symbol denotes the deviation of the geomagnetic field components from the nighttime level. The FRD station is located at 48.0° dipole-geomagnetic latitude, which is usually north of the northern Sq focus during the northern winter months [*Campbell and Schiffmacher*, 1986]. Before the peak reversal of the zonal wind (indicated by a vertical black line in Figure 1c), the daily variation of the geomagnetic field ΔH at FRD is characterized by negative values during the daytime hours, indicating westward currents flowing over the station. However, after the peak reversal of the zonal wind, the amplitude of the daily variation is very small and the daytime negative values in ΔH are barely visible. This change in the pattern of the geomagnetic daily variation is indicative of a decrease of the westward currents and/or a latitudinal shift of the Sq-focus position. The PST station is located at −41.7° dipole-geomagnetic latitude, which is usually south of or beneath the southern Sq focus [*Gupta*, 1973; *Campbell and Schiffmacher*, 1988]. Before the peak reversal of the zonal wind, the amplitude of the daily variation of the *H*-component geomagnetic field is small and the pattern is not consistent, which indicates that the station is very close to the latitude of the southern Sq focus. After the peak reversal of the zonal wind, a negative peak around noon is evident. The change in the pattern of the geomagnetic daily variation at PST indicates an increase of the westward currents and/or a latitudinal shift of the Sq-focus position.

[14] To provide some insight into lunar tidal activity during this period, we plot in Figure 1e the amplitude of the semimonthly component of the geomagnetic daily variation in ΔH at Huancayo (HUA). The HUA station is located near the geomagnetic equator, and hence ΔH is dominated by the effect of the equatorial electrojet. The semimonthly (or 14.76-day) Fourier component is determined on a daily basis, applying a 15-day sliding window to ΔH at each local time. Semimonthly modulation of the geomagnetic daily variation is well known and believed due in large part to ionospheric wind-dynamo currents driven by atmospheric lunar tides [*Tarpley*, 1970]. It has to be noted, however, that the semimonthly Fourier component can be affected by any variation that has similar periodicities with lunar tides. For example, 13 to 14 day periodicities in solar emissions [e.g., *Donnelly and Puga*, 1990] may be reflected in the electric conductivity of the E-region ionosphere and hence in ground magnetic field variations. In Figure 1e, one can see an enhancement of the semimonthly component around January 15 with an amplitude of 80 nT. At the same time an enhancement of the semimonthly component is also observed at FRD and PST but with much smaller amplitudes of approximately 15 nT (not shown here). The enhancement of the semimonthly component in the equatorial electrojet

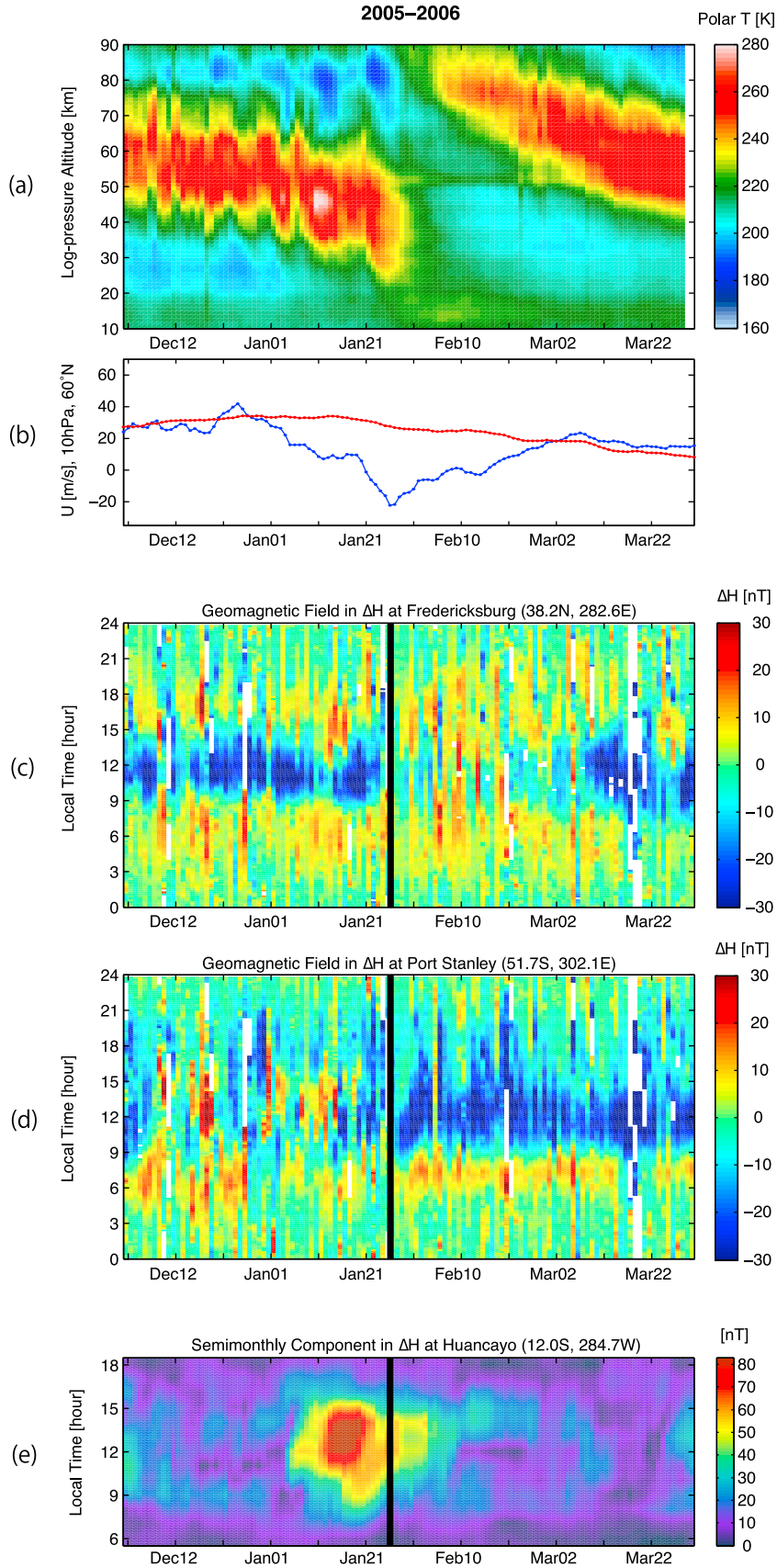
2005–2006
Polar T [K]
(a)
Log-pressure Altitude [km]
(b)
U [m/s], 10hPa, 60°N
(c)
Geomagnetic Field in ΔH at Fredericksburg (38.2N, 282.6E)
ΔH [nT]
Local Time [hour]
(d)
Geomagnetic Field in ΔH at Port Stanley (51.7S, 302.1E)
(e)
Semimonthly Component in ΔH at Huancayo (12.0S, 284.7W)
[nT]
Dec12
Jan01
Jan21
Feb10
Mar02
Mar22

Figure 1

during the January 2006 SSW event is consistent with a previous report by *Park et al.* [2012]. The simultaneous increase of the semimonthly component at the geomagnetic equator and at middle latitudes is probably due to a global enhancement of the lunar current system, as suggested by *Yamazaki et al.* [2012b].

[15] Figure 2 is the same as Figure 1 but for the winter months of 2008–2009. The reversal of the zonal wind at 10 hPa from eastward to westward, and the subsequent elevation of the stratopause altitude can be seen in Figures 2b and 2a, respectively. The conditions for a major SSW were satisfied on 24 January. Remarkable changes in the pattern of the geomagnetic daily variation at FRD and PST are observed around the peak reversal of the zonal wind on January 29, 2009 (indicated by vertical black lines in Figures 2c and 2d). The changes in the daily variation of the geomagnetic field are consistent with those of the January-2006 SSW event; a decrease and increase in the amplitude of the geomagnetic daily variation are observed at FRD and PST, respectively. Moreover, an enhancement of the semimonthly component of the geomagnetic daily variation in ΔH is observed at HUA with the maximum amplitude around the peak reversal of the stratospheric zonal wind (Figure 2e). The enhancement of the semimonthly component in the equatorial electrojet during the January-2009 SSW event was previously reported by *Park et al.* [2012].

3.2. Ionospheric Sq Current System During the SSW Events

[16] We have presented two types of changes in the daily geomagnetic field variation during unusually strong and prolonged SSW events in January 2006 and January 2009. One is long-lasting changes in the pattern of the geomagnetic daily variation at middle latitudes, as shown in Figures 1c, 1d, 2c and 2d. The other is the enhancement of the semimonthly component of the geomagnetic daily variation, as shown in Figures 1e and 2e. The latter can be attributed to a global enhancement of the luni-solar (L) current system, whose geomagnetic effects have been already established in the past [*Yamazaki et al.*, 2012a, 2012b]. Therefore, our analysis of the ionospheric current system focuses only on the former.

[17] Ionospheric current systems are estimated based on a spherical harmonic analysis of the geomagnetic daily variations. The method of data processing is the same as that used in our previous study [*Yamazaki et al.*, 2012b], and thus only briefly outlined here. Geomagnetic daily variations observed along a north-south chain of stations are used. All three components of the geomagnetic field H, D, and Z are included in the analysis. Data for periods of high magnetic activity ($Kp > 3+$) are eliminated from the data set. A magnetic potential of the geomagnetic daily variation is determined in geomagnetic-latitude versus local-time coordinates under the assumption that longitude and local time are equivalent. Following standard techniques [e.g., *Campbell*, 2003], external and internal Gauss coefficients of the spherical harmonic expansion of the magnetic potential are determined, and equivalent ionospheric (external) current systems hypothetically flowing in a thin spherical shell at an altitude of 110 km are derived.

[18] Figure 3 shows current functions of the ionospheric Sq current system for different periods obtained from the American magnetometer chain. Each current system is derived from the geomagnetic daily variation averaged over 15 days. This averaging period was selected so that geomagnetic effects due to the L current system would be canceled out or minimized. In the figure, equivalent currents flow along contour lines with steps of 25 kA between adjacent contours. The direction of the flow is counterclockwise around a positive peak and clockwise around a negative peak. A current pattern with a counterclockwise vortex in the Northern Hemisphere and a clockwise vortex in the Southern Hemisphere is a robust feature of the Sq current system [e.g., *Pedatella et al.*, 2011; *Yamazaki et al.*, 2011]. The Sq current systems have been calculated for the period from December to March of 2004–2005, 2005–2006, and 2008–2009. In the following paragraphs, we present the results only for December and February of each winter period, which illustrate the essential features that we have found.

[19] We first look at the Sq current systems observed during the northern winter months of 2004–2005, when no SSW event was recorded. Figures 3a and 3b show the Sq current systems for late December of 2004 and middle February of 2005, respectively. Some features can be commonly seen in these figures. First, the current intensity is greater in the Southern Hemisphere. Secondly, the southern current focus is located at an earlier local time than the northern counterpart. Thirdly, the southern current system penetrates into the Northern Hemisphere during the morning hours, crossing the geomagnetic equator. The first feature arises from the fact that the electric conductivity is greater in the local summer hemisphere due to higher solar zenith angle. The second and third features are considered to result from the north-south asymmetry of the ionospheric dynamo due to anti-symmetric wind distributions. Previous studies have shown that field-aligned magnetospheric currents as well as ionospheric currents contribute to these features [*Schieldge et al.*, 1973; *Takeda*, 1990; *Le Sager and Huang*, 2002]. Since our Sq current systems are derived under the assumption that currents are flowing in a thin spherical shell, it is not possible to separate magnetospheric and ionospheric contributions.

Figure 1. An overview of the SSW event in January 2006. (a) A height-time section of the polar cap temperature (northward of 70 degree) based on MLS observations from December 2005 through March 2006. The color bar shows temperature contours in K. The vertical axis denotes log pressure altitude, $z_p = H \ln 1000/p$, where $H = 7$ km and p is pressure in hPa. (b) The zonal mean zonal wind at 60°N based on the NCEP-NCAR reanalysis from December 2005 through March 2006 (blue) with the corresponding climatological seasonal cycle (red). (c) Daily variations of the geomagnetic field ΔH at Fredericksburg (FRD). The vertical axis denotes solar local time in hours. Periods of high magnetic activity ($Kp > 3+$) are shown in white. (d) Same as Figure 1c but for Port Stanley (PST). (e) The amplitude of the semimonthly component of the geomagnetic daily variation in ΔH at Huancayo (HUA). See text for details.

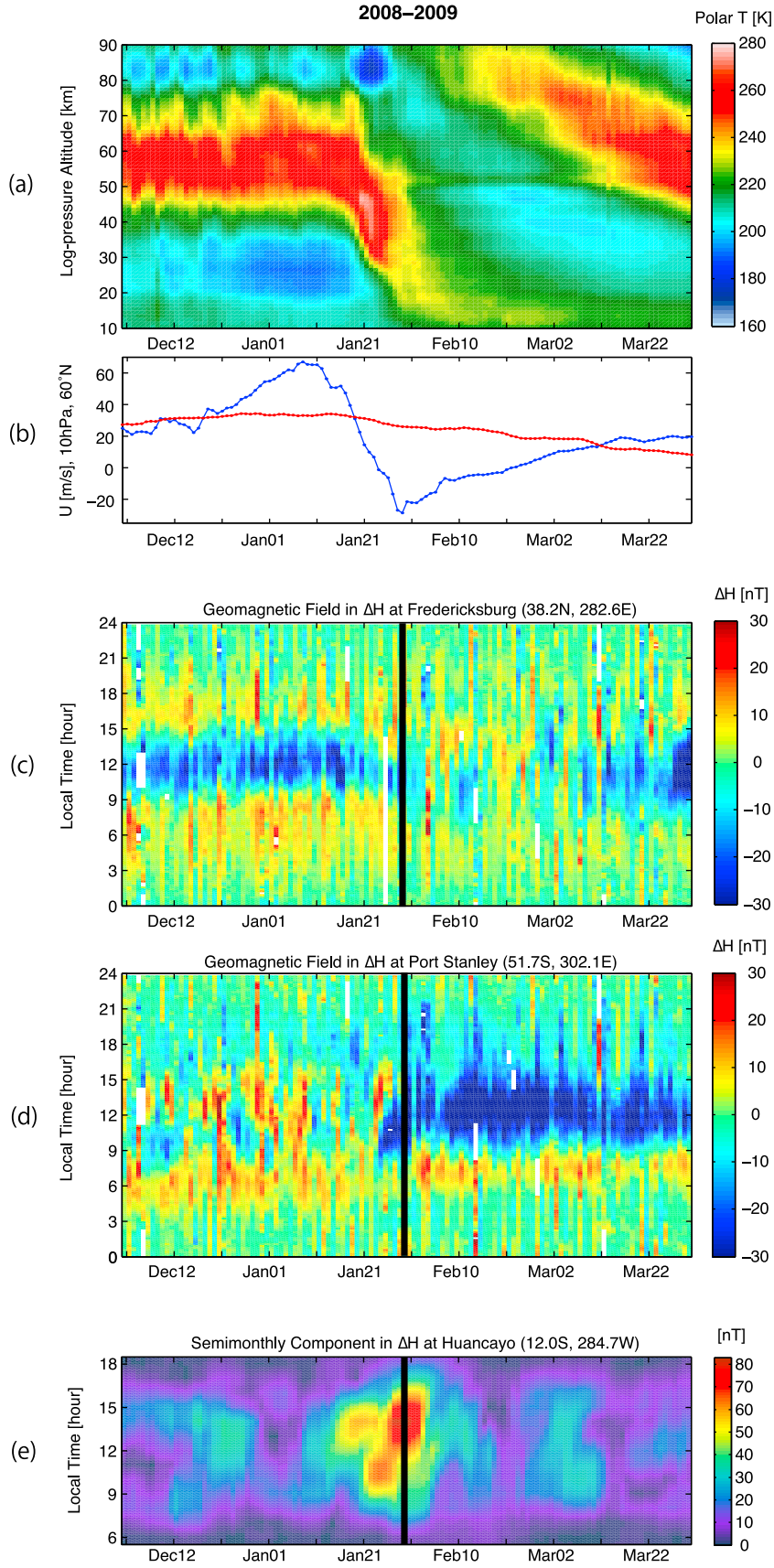

Figure 2. Same as Figure 1, but for the SSW event in January 2009.

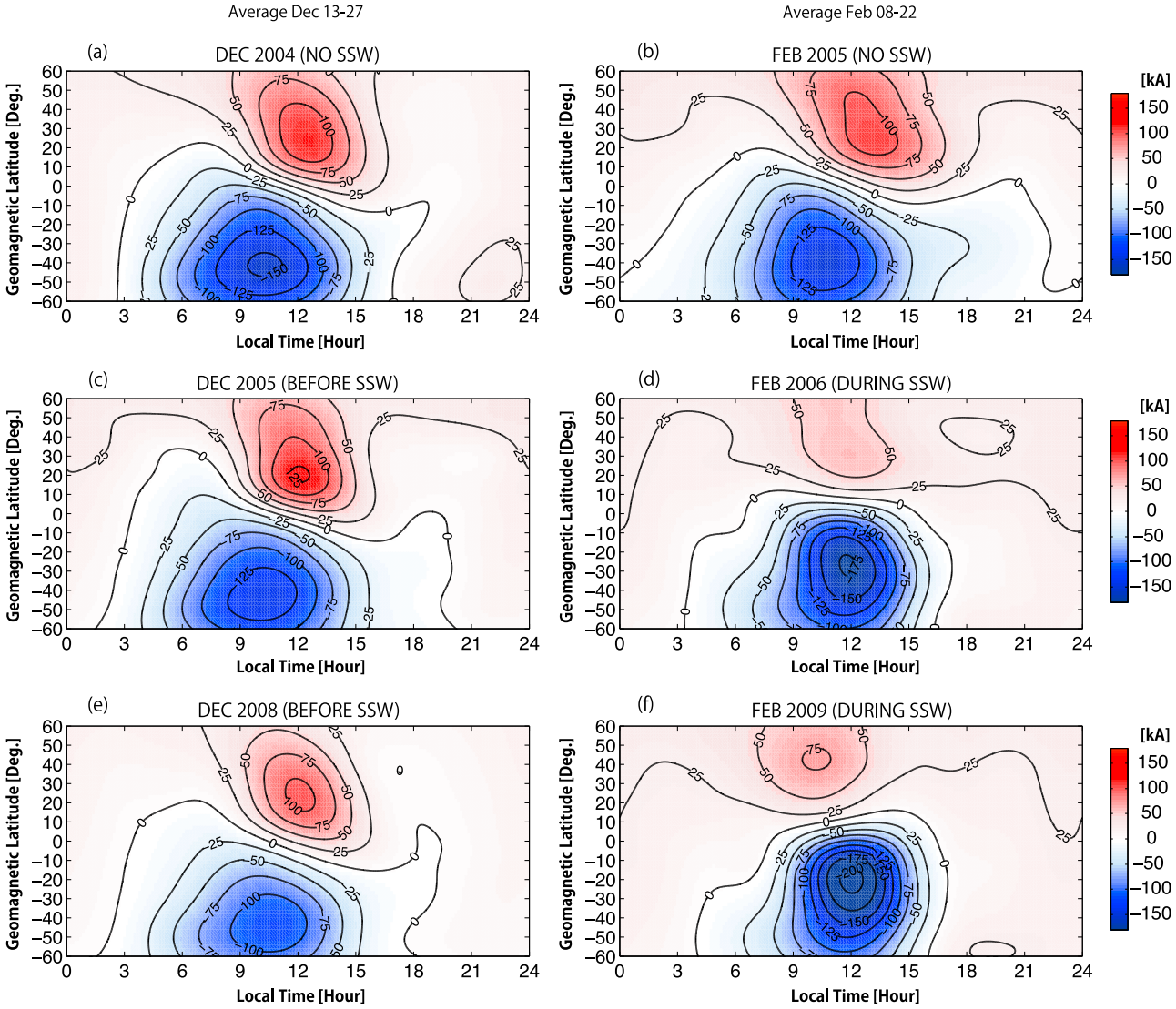

Figure 3. Sq current functions derived from ground-magnetometer data at the American sector for (a) late December of 2004, (b) middle February of 2005, (c) late December of 2005, (d) middle February of 2006, (e) late December of 2008, and (f) middle February of 2009. Current flow contours are drawn with 25 kA steps in latitude versus local time coordinates.

[20] Figures 3c and 3e are the same as Figure 3a but for the years 2005 and 2008, respectively, showing ionospheric Sq current systems before the start of the SSW events (see also Figures 1 and 2). All the features described above can be confirmed. The current intensity is greater in December 2005 than December 2008. This is explained as a solar-activity effect: higher solar activity leads to higher ionospheric conductivity, allowing stronger currents to flow [*Takeda et al.*, 2003]. Monthly averaged values of the solar-activity index $F10.7$ (in a unit of 10^{-22} Wm^{-2} Hz^{-1}) is 82 for December 2005 and 67 for December 2008.

[21] Figures 3d and 3f are the same as Figure 3b but for the years 2006 and 2009, respectively, displaying ionospheric Sq current systems during the SSW events (see also Figures 1 and 2). In comparison with the current systems before the SSW, the following features can be noticed: (1) the southern current intensity is greater (by 40% for the 2006 event and by 70% for the 2009 event), while the northern current intensity is weaker by 50% for the 2006 event and by 30% for the 2009 event, (2) the southern current focus is located at a later local time, while the northern current focus is located at an earlier local time, and (3) the penetration of the southern current system into the Northern Hemisphere during the morning hours between 6 and 10 local time is reduced. These features are not explained by seasonal changes in the ionospheric conductivity, and thus are probably due to changes in the wind system in the dynamo region of the ionosphere.

[22] There are significant differences between the ionospheric Sq current systems before and during the SSW events. To illustrate this effect, we show in Figure 4 current vectors for the differences. The current pattern is not obvious in Figure 4a, which displays the results of the non-SSW year (February 2005 minus December 2004). On the other hand, the results of the SSW years in Figures 4b and 4c (February

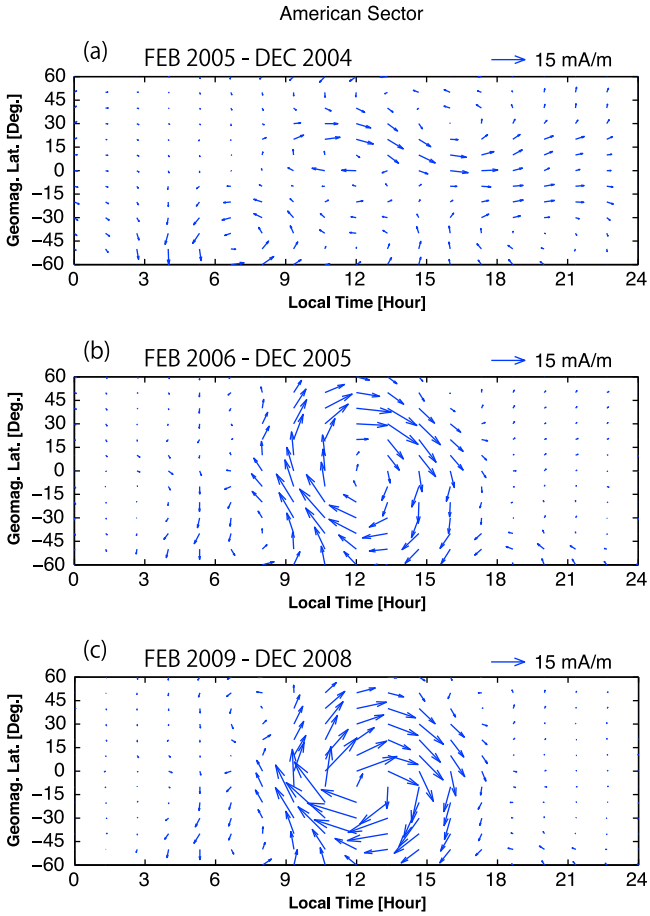

Figure 4. Current vectors at the American sector for (a) February 2005 minus December 2004, (b) February 2006 minus December 2005, and (c) February 2009 minus December 2008.

2006 minus December 2005 and February 2009 minus December 2008, respectively) reveal a single clockwise vortex centered around the noon at the magnetic equator. It is interesting to note that the current patterns in both Figures 4b and 4c are semidiurnal, extending in local time from 09:00 to 16:00.

[23] Figure 5 is the same as Figure 4c except that the data from the Asian sector are used (see Table 1). It can be seen in Figure 5 that the current pattern is similar to that observed at the American sector (Figure 4c), showing a semidiurnal clockwise vortex extending in local time from 09:00 to 16:00. This confirms our early results, where we reported the amplification of the southern Sq current system with disappearance of the northern current vortex at the Asian sector during the January-2009 SSW event [*Tanaka et al.*, 2009]. For the January-2006 SSW event, it was not possible to deduce the Sq current system in the Asian longitude sector because of a lack of global data. Nonetheless, the geomagnetic daily variation at individual stations indicated a decrease and increase of the northern and southern Sq current intensities, respectively, which is consistent with the results at the American longitude. The consistency of the current pattern at American and Asian longitudes suggests the importance of migrating tidal effects. The current intensity is, however, weaker at the Asian sector, indicating weaker effects of the SSW (see Figures 4c and 5). A possible reason for the weaker effect at the Asian sector is the stronger background magnetic field in the Asian region than the American region. A stronger background magnetic field leads to lower ionospheric conductivity [e.g., *Shinbori et al.*, 2010]. Note that longitude differences in the patterns mean that the assumption used in our method of equivalence between longitudinal and local-time variations is not strictly valid. Nevertheless, the longitude differences are relatively small in comparison with the differences between periods with or without SSW, which gives us confidence that the basic features of the Sq patterns in these figures are valid.

3.3. Role of Solar Migrating Semidiurnal Tides

[24] Solar migrating semidiurnal tides are mainly excited in the troposphere and stratosphere, and then propagate upward to the ionosphere. Since their propagation properties are strongly dependent on the state of the background wind and temperature, these tides might be affected by circulation changes in the middle atmosphere during the SSW events. Also, changes in stratospheric ozone during the SSW events might cause changes of the solar tide. In this part of the paper, a mechanistic study is made to investigate if it is possible for solar migrating semidiurnal tides to explain the observed SSW effects on the Sq current system, and if so, which tidal mode is responsible.

[25] We carry out numerical simulations using the NCAR/TIE-GCM. At the lower boundary of the model (approximately 97 km altitude), the amplitudes and phases of solar migrating diurnal and semidiurnal tides can be specified by the Global Scale Wave Model (GSWM) [*Hagan and Forbes*, 2002, 2003]. (Note that the background atmosphere in the GSWM is climatological and thus does not include SSW effects. Also note that non-migrating tides are neglected in our simulations.) In the present study, the geopotential, wind and temperature fields from the February GSWM results at the altitude of the TIEGCM lower boundary are decomposed into the following Hough modes in accordance with classical tidal theory [e.g., *Lindzen and Chapman*, 1969]: (1,1), (2,2), (2,3), (2,4), (2,5) modes. Other higher-degree modes of diurnal and semidiurnal solar migrating tides are found to be much smaller in amplitude, and hence they are neglected in this study. Our numerical experiments described in the following paragraphs aim to find out which Hough mode could be important in producing the observed changes in the Sq current system during the SSW events.

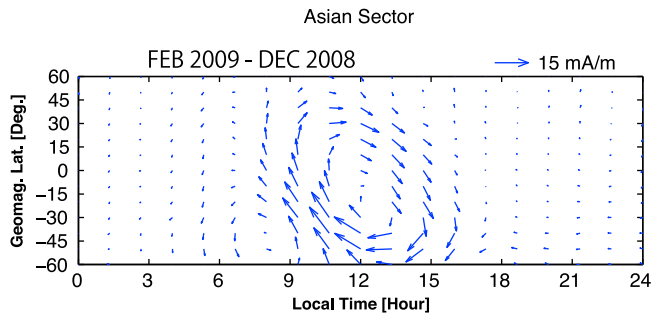

Figure 5. Same as Figure 4c, but at the Asian sector.

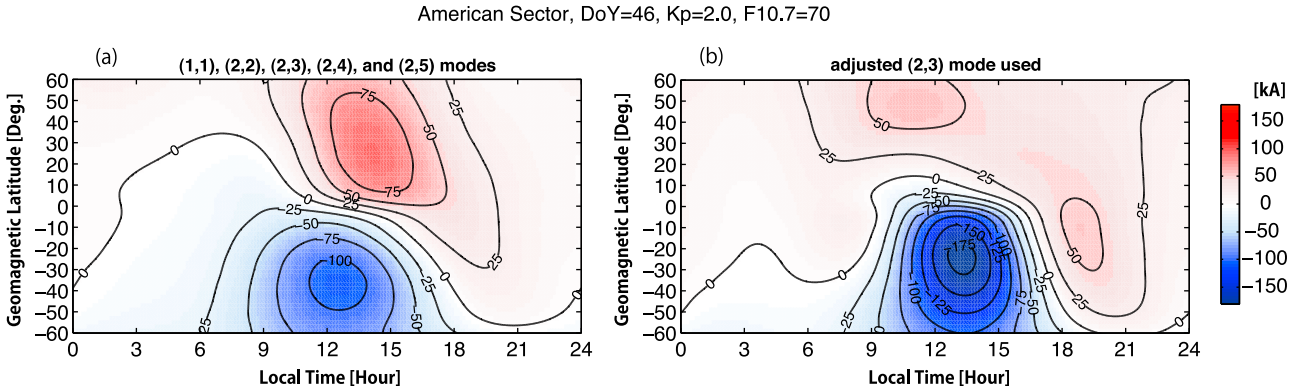

Figure 6. Sq current functions at the American sector (355-degree E magnetic longitude) simulated by the NCAR/TIE-GCM for solar-minimum February conditions (*DoY* = 46, *Kp* = 2.0, and *F*10.7 = 70), (a) with (1,1), (2,2), (2,3), (2,4), (2,5) modes from the GSWM at the lower boundary, and (b) with (1,1), (2,2), (2,4), (2,5) modes from the GSWM and the adjusted (2,3) mode at the lower boundary. See text for details of the adjusted (2,3) mode.

[26] Figure 6a shows the ionospheric Sq current system obtained from a steady state simulation of the NCAR/TIE-GCM. For comparison with the observation results, we first calculated geomagnetic daily variations at model grid points along the 355° magnetic meridian, which is approximately the 75°W (American) geographic meridian, under geomagnetically quiet conditions. We then derived the ionospheric Sq current system using the same fitting procedure as used for the observations in Section 3.2. The current system in Figure 6a well reproduces the main features of that observed in February of the non-SSW year 2005 (see Figure 3b). The current intensity is greater in the Southern Hemisphere than the Northern Hemisphere, and the southern current focus is located at an earlier local time. Also, intrusion of the southern current system into the Northern Hemisphere during the morning hours is visible.

[27] Quantitative agreement between the model and observation results justifies further evaluation of the role of each tidal mode in producing the ionospheric Sq current system. In order to characterize the tidal effects, ionospheric current systems are derived from the NCAR/TIE-GCM with different tidal inputs at the lower boundary. We first calculated the ionospheric current system without tidal forcing at the lower boundary. In this simulation, the currents are mainly driven by the locally generated tide, which is known as the main driver of the ionospheric Sq current system [*Takeda and Maeda*, 1980]. The derived current system is shown in Figure 7. One can see that the current pattern is essentially the same as that in Figure 6a, showing counterclockwise and clockwise vortices in the Northern and Southern Hemispheres, respectively. The current intensity accounts for approximately 80% of that in Figure 6a; in other words, contributions of upward-propagating tides from the lower boundary are approximately 20%.

[28] Figures 8a–8d show ionospheric current systems for different solar migrating semidiurnal tides. The current systems are first calculated with tidal forcing of each mode at the lower boundary, and then the results of the base case in Figure 7 are subtracted to isolate the effects of the lower-boundary tides. Note that the scale of current vectors in Figure 8 is one fifth of that in Figure 7. It is seen that the current systems produced by the (2,2) mode (Figure 8a) and (2,4) mode (Figure 8c) have a counterclockwise vortex in the Northern Hemisphere and a clockwise vortex in the Southern Hemisphere, as does the base-case Sq current system in Figure 7. Therefore, these modes from the GSWM act to simultaneously increase northern and southern current intensities. This is not surprising when one considers that both the (2,2) mode and (2,4) mode are "symmetric tides". For symmetric tides the eastward wind velocity u is symmetric with respect to the geographic equator and the northward wind velocity v changes the sign at the equator. On the other hand, the (2,3) mode and (2,5) modes are "anti-symmetric tides", for which v is symmetric with respect to the geographic equator and u changes the sign at the equator. Although the difference between geographic and magnetic coordinates means that geographically (anti)symmetric tides are not entirely (anti)symmetric in magnetic coordinates, the symmetric or antisymmetric properties of the tides still tend to dominate even after coordinate transformation.

[29] The current system produced by the (2,3) mode is shown in Figure 8b. The equivalent currents are dominated by a vortex with flow across the geomagnetic equator, which extends between 10 and 17 local time with southward

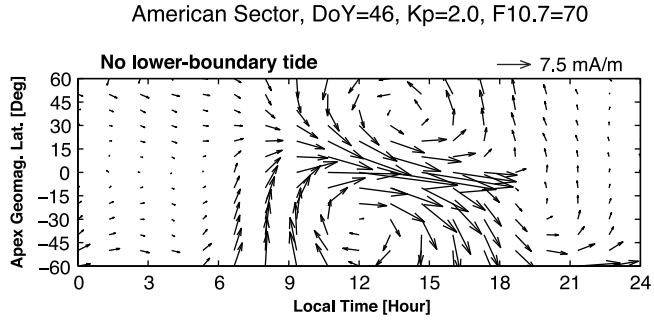

Figure 7. Current vectors at the American sector simulated by the NCAR/TIE-GCM without tides at the lower boundary.

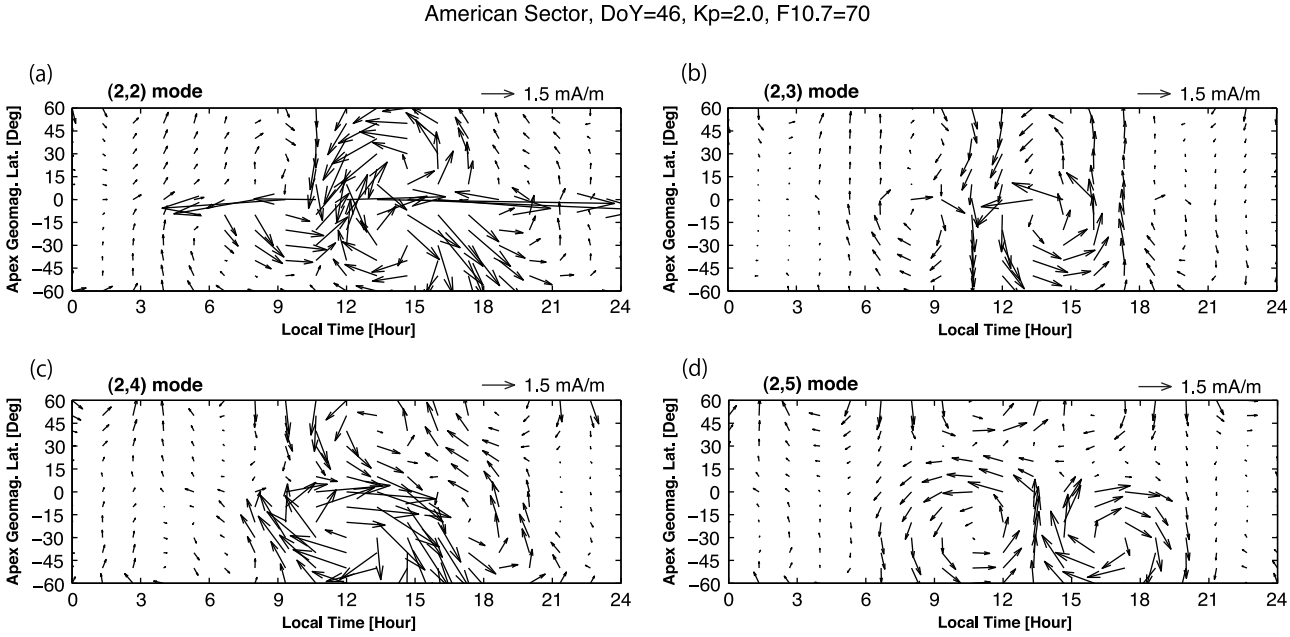

Figure 8. Current vectors at the American sector simulated by the NCAR/TIE-GCM, showing effects of (a) the (2,2) mode, (b) the (2,3) mode, (c) the (2,4) mode, and (d) the (2,5) mode from the GSWM at the lower boundary.

currents in the morning and northward currents in the afternoon. This current pattern is similar to those in Figures 4b and 4c, but the direction of the current flow is opposite. Recalling that the clockwise current systems in Figures 4b and 4c are equivalent to a decrease of the northern Sq current intensity and an increase of the southern Sq current intensity, it is understood that the counter-clockwise current system by the GSWM (2,3) mode increases the northern current intensity and decreases the southern current intensity of the base-case Sq current system in Figure 7. A current system that has the same current pattern as in Figure 8b but in a clockwise direction can be readily obtained by changing the phase of the (2,3) mode at the lower boundary by 6 hours. Although the (2,5) mode is also an anti-symmetric tide, the current system for the (2,5) mode (Figure 8d) is quite different from that for the (2,3) mode, showing additional current vortices above 30° latitude that are reversed in direction from the larger vortices to the south.

[30] As is shown above, the (2,3) mode can increase the current intensity of one hemisphere and, at the same time, decrease the current intensity of the other hemisphere. Therefore, by adjusting the amplitude and phase of the (2,3) mode at the lower boundary of the model, it is possible to produce an ionospheric current system similar to those observed during the SSW events (Figures 3d and 3f). Figure 6b shows the ionospheric Sq current system obtained from a NCAR/TIE-GCM simulation. In this simulation, the initial conditions are the same as those in Figure 6a except that the amplitude of the (2,3) mode at the lower boundary is increased by a factor of 6 and the phase of the (2,3) mode is shifted by 6 hours. (The 6-hour phase shift means that the wind pattern is the opposite of that in the February-GSWM results.) The (2,3) mode used here is referred to as the "adjusted (2,3) mode" from now on. From the comparison between Figures 6a and 6b, one can see that the adjusted (2,3) mode leads to the following changes: (1) the southern current intensity is increased by 70%, while the northern current intensity is decreased by 40%, (2) the southern current focus is shifted to a later local time, while the northern current focus is shifted to an earlier local time, and (3) the penetration of the southern current system into the Northern Hemisphere during the morning hours is reduced. These changes are very similar to those observed during SSW events.

[31] The height profile of the adjusted (2,3) mode at 45° latitude, along with ionospheric conductivities, is shown in Figure 9. It can be seen that the amplitude of the adjusted (2,3) mode reaches its maximum at approximately 120 km altitude. The peak amplitude of 50–60 m/s is large, but not unrealistically so, for the tidal amplitude at these altitudes. The height variation of phase in Figure 9b shows downward phase progression with increasing time, which is characteristic of tides with upward energy flux. u lags three hours behind v, meaning that the wind vector rotates clockwise in time, which is typical of tides at most locations in the Northern Hemisphere. The vector also rotates clockwise with increasing height. (In the Southern Hemisphere the sense of rotation is opposite to that in the Northern Hemisphere, because of the opposite directions of Coriolis acceleration in the two hemispheres.) Figures 10a and 10b show the latitude local time distributions of the wind vectors for the adjusted (2,3) mode at 115 and 135 km altitudes, respectively. As is seen in Figure 9c, at 115 km the Hall conductivity is greater than the Pedersen conductivity, while at 135 km the Pedersen conductivity is predominant. According to wind-dynamo theory, the Hall current $\mathbf{J}_H$ and the Pedersen current $\mathbf{J}_P$ are described as follows:

$$\mathbf{J}_H = \sigma_H \mathbf{b} \times (\mathbf{E}_\perp + \mathbf{v} \times \mathbf{B}) \quad (1)$$

$$\mathbf{J}_P = \sigma_P (\mathbf{E}_\perp + \mathbf{v} \times \mathbf{B}) \quad (2)$$

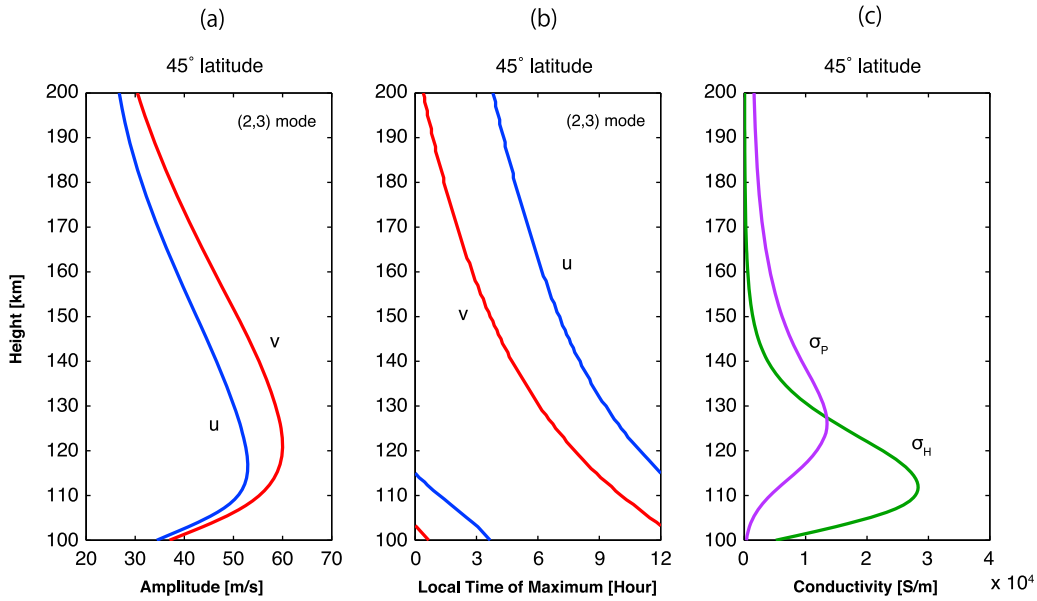

Figure 9. (a) Amplitudes of the eastward (blue) and northward (red) components at 45° latitude for the adjusted (2,3) mode. (b) Phases of the eastward (blue) and northward (red) components at 45° latitude for the adjusted (2,3) mode. (c) Hall conductivity (green) and Pedersen conductivity (purple) at 45° latitude at local noon.

where **b** is a unit vector in the direction of the geomagnetic field **B**; $\mathbf{E}_\perp$ is the electric field perpendicular to **B**; **v** is the wind velocity. The Hall current and Pedersen current together with the current parallel to the geomagnetic field form a three dimensional current closure. The electric field produced by the dynamo action of the wind is electrostatic, for which the electric potential is nearly constant along geomagnetic field lines all the way from the bottom of the ionosphere in one hemisphere to the bottom of the ionosphere in the opposite hemisphere. That is, the electric field is constrained to be approximately symmetric about the magnetic equator. Antisymmetric dynamo action produced by winds that are antisymmetric about the (magnetic) equator is ineffective in generating an electric field, although such winds can drive electric current. The (2,3) mode is antisymmetric about the geographic equator, but is not exactly antisymmetric about the magnetic equator. Nevertheless, it is relatively ineffective in generating an electric field, in

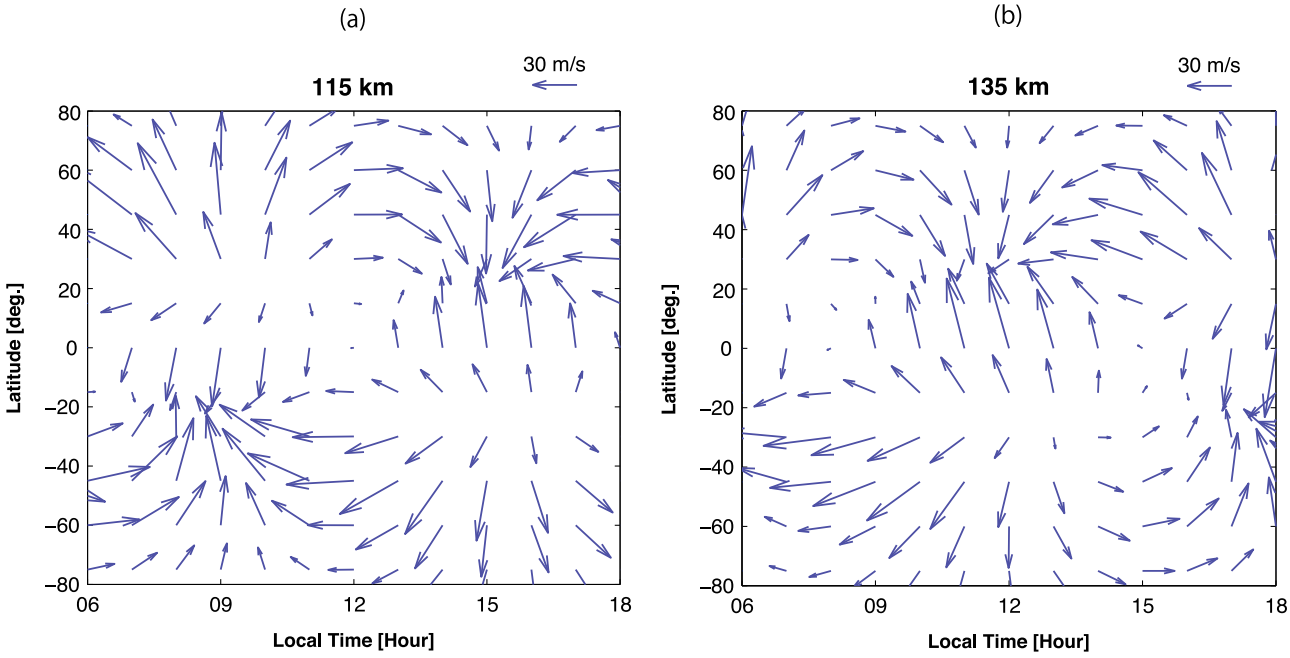

Figure 10. Wind vectors for the adjusted (2,3) mode at (a) 115 km altitude, and (b) 135 km altitude.

comparison with the fields generated by hemispherically symmetric winds such as the (2,2) tidal mode. Therefore, to understand the basic properties of currents driven by the (2,3) mode we can ignore the electric field in (1)–(2).

[32] Neglecting the vertical component of **v**, the horizontal components (eastward and northward components) of $\mathbf{J}_H$ are proportional to $\sigma_H B_z(u, v)$ in the Northern Hemisphere (where downward geomagnetic field $B_z > 0$) and to $-\sigma_H B_z(u, v)$ in the Southern Hemisphere (where $B_z < 0$). Therefore, the horizontal component of $\mathbf{J}_H$ flows in the direction of the horizontal wind, as it represents current carried by positive ions that are largely entrained by the wind. On the other hand, the horizontal components of $\mathbf{J}_P$ are proportional to $\sigma_P B_z(v, -u)$ in both hemispheres. $\mathbf{J}_P$ flows in a direction rotated 90° counterclockwise from the wind direction in the Northern Hemisphere (where $B_z > 0$) and 90° clockwise in the Southern Hemisphere (where $B_z < 0$). The magnitude of the currents depends on the ionospheric conductivities, strength of the geomagnetic field, and wind speed. σ_P and σ_H are small at high latitudes because of the strong geomagnetic field, as well as lower ionizing solar fluxes than at low latitudes. Meanwhile, B_z is small at the low latitude regions and tends to increase with increasing latitude. Therefore, the midlatitude regions tend to be particularly effective for the generation of global current (the wind is also relatively large there).

[33] Keeping the facts mentioned in the previous paragraph in mind, we can now understand why the adjusted (2,3) mode decreases northern Sq currents and increases southern Sq currents. At 115 km altitude, where $\sigma_H > \sigma_P$, winds due to the (2,3) mode at middle latitudes (30 to 60 degrees) are mainly eastward in the Northern Hemisphere and westward in the Southern Hemisphere for 10 to 15 local time when the ionospheric conductivities are most significant (Figure 10a). Accordingly, eastward Hall currents are driven in the Northern Hemisphere, which tend to reduce the normal Sq currents in the Northern Hemisphere that are westward at middle latitudes (Figure 3). Also, westward Hall currents are driven in the Southern Hemisphere, which tend to strengthen the normal Sq currents in the Southern Hemisphere that are westward at middle latitudes (Figure 3). The meridional closure of the westward northern and eastward southern currents driven by the adjusted (2,3) tide occurs to a large extent by currents flowing parallel to the geomagnetic field, both within the ionosphere and above the ionosphere.

[34] It so happens that Pedersen currents at higher altitudes tend to reinforce the effects of the Hall currents, owing to the rotation of the wind direction with height of the (2,3) mode. At 135 km altitude, where $\sigma_P > \sigma_H$, the midlatitude winds around noon are mainly southward in both the Northern and Southern Hemispheres (Figure 10b). Accordingly, eastward Pedersen currents are driven in the Northern Hemisphere, which tend to reduce the normal Sq currents in the Northern Hemisphere that are westward at midlatitudes. Also, westward Pedersen currents are driven in the Southern Hemisphere, which tend to strengthen the normal Sq currents in the Southern Hemisphere that is westward at midlatitudes. Therefore, the currents driven by the adjusted (2,3) mode tend to reduce the northern Sq current system and strengthen the southern Sq current system throughout the dynamo region of the ionosphere.

[35] Our results suggest that changes in the solar (2,3) semidiurnal mode from below the ionosphere can cause the unusual Sq current system during the SSW events. The modulation of upward propagation of the atmospheric tide due to changes in wind and temperature fields during the SSW events could be a reason for such tidal changes. Changes in stratospheric ozone during the SSW events could also be a reason for the tidal changes. It is known that an asymmetric distribution of stratospheric ozone with respect to the equator can excite the (2,3) mode [*Teitelbaum and Cot*, 1979]. *Goncharenko et al.* [2012] showed an increase in the zonal mean ozone, lasting for more than one month, during the January-2009 SSW event. The impact of stratospheric ozone changes on the (2,3) mode during the SSW events remains to be studied. The interaction between planetary waves and tides could also cause tidal changes in the ionosphere, but most significantly in non-migrating tides [*Liu et al.*, 2010]. The fact that the SSW effects in the equivalent current system in America and East Asia are similar argues in favor of a migrating tidal source. Other possibilities such as changes in locally generated tides and mean winds also need to be verified by further observations or model simulations.

[36] Finally, if changes in the solar (2,3) semidiurnal mode are caused by changes in the background fields during SSW events, similar changes will be produced in the lunar (2,3) semidiurnal mode. Although the Sq current systems we have shown in this study are derived on the basis of the 15-day average so that lunar contributions will be minimized, the actual day-to-day changes in the currents that occur during SSW events will contain both the lunar- and solar-driven changes. It is known that the pattern of the lunar current system during the northern winter months is sometimes highly asymmetric with respect to the geomagnetic equator [*Matsushita and Xu*, 1984], which may possibly be due to the enhanced lunar (2,3) semidiurnal mode during SSW events. Possible changes in the lunar anti-symmetric tide during SSW events and its impact on the ionospheric wind-dynamo also need to be clarified.

4. Summary

[37] Our analysis of the INTERMAGNET data has revealed significant changes in the ionospheric Sq current system during unusually strong and prolonged stratospheric sudden warming (SSW) events in January 2006 and January 2009 (Figures 1 and 2). The observed changes are characterized by a decrease and increase of the Sq current intensity in the Northern and Southern Hemispheres, respectively (Figure 3). The effects are equivalent to the addition of a semidiurnal clockwise current system centered around noon at the magnetic equator (Figures 4 and 5). Numerical experiments using the NCAR/TIE-GCM have demonstrated that an anti-symmetric (2,3) semidiurnal mode from below the ionosphere can cause similar effects on the ionospheric current system (Figures 6, 7 and 8). The Sq current system during the SSW events could be produced by using a large-amplitude (2,3) mode (50–60 m/s in the dynamo region) with a particular phase (Figures 9 and 10), the existence of which, however, remains to be confirmed by further observations and/or simulations. Possible mechanisms other than the (2,3) mode also need to be evaluated in future studies.

[38] **Acknowledgments.** We are thankful to Astrid Maute for her assistance in the NCAR/TIE-GCM simulations, and to Nick Pedatella for comments on a draft of this paper. We are also thankful to Maura Hagan for providing the GSWM fields decomposed into Hough modes. The results presented in this paper rely on data collected at magnetic observatories. We thank the national institutes that support them and INTERMAGNET for promoting high standards of magnetic observatory practice. We also thank GSI Geomagnetic Survey for providing the geomagnetic data collected at Okinawa, and the OHP DMC for providing the geomagnetic data collected at Ponape. We acknowledge the National Institute of Information and Communications Technology for providing the magnetometer data for our initial study. We are grateful to the MLS science team for processing and distributing the satellite data. We are also grateful to NOAA/OAR/ESRL PSD, Boulder, Colorado, for providing NCEP-NCAR reanalysis data. The magnetic activity index *Kp* is provided by the German Research Center for Geosciences (GFZ). The solar activity index *F*10.7 is provided by the Herzberg Institute of Astrophysics. Y.Y. was supported by a Research Fellowship of the Japan Society for the Promotion of Science (JSPS) for Research Abroad. H.L. was partly supported by a Grant-in-Aid for Scientific Research (23540513) from the Ministry of Education, Culture, Sports, Science and Technology, Japan. The National Center for Atmospheric Research is sponsored by the National Science Foundation.

[39] Robert Lysak thanks the reviewers for their assistance in evaluating this paper.

References

Anderson, D., and E. A. Araujo-Pradere (2010), Sudden stratospheric warming event signatures in daytime $\mathbf{E} \times \mathbf{B}$ drift velocities in the Peruvian and Philippine longitude sectors for January 2003 and 2004, *J. Geophys. Res.*, *115*, A00G05, doi:10.1029/2010JA015337.

Andrews, D., J. R. Holton, and C. B. Leovy (1987), Stratospheric sudden warmings, in *Middle Atmosphere Dynamics*, pp. 259–294, Elsevier, New York.

Campbell, W. H. (2003), *Introduction to Geomagnetic Fields*, 2nd ed., 102 pp., Cambridge Univ. Press, Cambridge, U. K.

Campbell, W. H., and E. R. Schiffmacher (1986), Correction to "Quiet ionospheric currents of the Northern Hemisphere derived from geomagnetic field records," *J. Geophys. Res.*, *91*(A8), 9023–9024, doi:10.1029/JA091iA08p09023.

Campbell, W. H., and E. R. Schiffmacher (1988), Quiet ionospheric currents of the Southern Hemisphere derived from geomagnetic records, *J. Geophys. Res.*, *93*(A2), 933–944, doi:10.1029/JA093iA02p00933.

Chandran, A., R. L. Collins, R. R. Garcia, and D. R. Marsh (2011), A case study of an elevated stratopause generated in the Whole Atmosphere Community Climate Model, *Geophys. Res. Lett.*, *38*, L08804, doi:10.1029/2010GL046566.

Chau, J. L., B. G. Fejer, and L. P. Goncharenko (2009), Quiet variability of equatorial $\mathbf{E} \times \mathbf{B}$ drifts during a stratospheric warming event, *Geophys. Res. Lett.*, *36*, L05101, doi:10.1029/2008GL036785.

Chau, J. L., N. A. Aponte, E. Cabassa, M. P. Sulzer, L. P. Goncharenko, and S. A. González (2010), Quiet time ionospheric variability over Arecibo during sudden stratospheric warming events, *J. Geophys. Res.*, *115*, A00G06, doi:10.1029/2010JA015378.

Chau, J. L., L. P. Goncharenko, B. G. Fejer, and H.-L. Liu (2011), Equatorial and low latitude ionospheric effects during sudden stratospheric warming events, *Space Sci. Rev.*, *168*(1–4), 385–417, doi:10.1007/s11214-011-9797-5.

de la Torre, L., R. R. Garcia, D. Barriopedro, and A. Chandran (2012), Climatology and characteristics of stratospheric sudden warmings in the Whole Atmosphere Community Climate Model, *J. Geophys. Res.*, *117*, D04110, doi:10.1029/2011JD016840.

Donnelly, R. F., and L. C. Puga (1990), Thirteen-day periodicity and the center-to-limb dependence of UV, EUV, and X-ray emission of solar activity, *Sol. Phys.*, *130*, 369–390.

Doumbia, V., A. Maute, and A. D. Richmond (2007), Simulation of equatorial electrojet magnetic effects with the thermosphere-ionosphere-electrodynamics general circulation model, *J. Geophys. Res.*, *112*, A09309, doi:10.1029/2007JA012308.

Fang, T. W., A. D. Richmond, J. Y. Liu, A. Maute, C. H. Lin, C. H. Chen, and B. Harper (2008), Model simulation of the equatorial electrojet in the Peruvian and Philippine sectors, *J. Atmos. Sol. Terr. Phys.*, *70*, 2203–2211.

Fejer, B. G., M. E. Olson, J. L. Chau, C. Stolle, H. Lühr, L. P. Goncharenko, K. Yumoto, and T. Nagatsuma (2010), Lunar-dependent equatorial ionospheric electrodynamic effects during sudden stratospheric warmings, *J. Geophys. Res.*, *115*, A00G03, doi:10.1029/2010JA015273.

Fejer, B. G., B. D. Tracy, M. E. Olson, and J. L. Chau (2011), Enhanced lunar semidiurnal equatorial vertical plasma drifts during sudden stratospheric warmings, *Geophys. Res. Lett.*, *38*, L21104, doi:10.1029/2011GL049788.

France, J. A., V. L. Harvey, C. E. Randall, M. H. Hitchman, and M. J. Schwartz (2012), A climatology of stratopause temperature and height in the polar vortex and anticyclones, *J. Geophys. Res.*, *117*, D06116, doi:10.1029/2011JD016893.

Fuller-Rowell, T., F. Wu, R. Akmaev, T.-W. Fang, and E. Araujo-Pradere (2010), A whole atmosphere model simulation of the impact of a sudden stratospheric warming on thermosphere dynamics and electrodynamics, *J. Geophys. Res.*, *115*, A00G08, doi:10.1029/2010JA015524.

Fuller-Rowell, T., H. Wang, R. Akmaev, F. Wu, T.-W. Fang, M. Iredell, and A. Richmond (2011), Forecasting the dynamic and electrodynamic response to the January 2009 sudden stratospheric warming, *Geophys. Res. Lett.*, *38*, L13102, doi:10.1029/2011GL047732.

Goncharenko, L. P., J. L. Chau, H.-L. Liu, and A. J. Coster (2010a), Unexpected connections between the stratosphere and ionosphere, *Geophys. Res. Lett.*, *37*, L10101, doi:10.1029/2010GL043125.

Goncharenko, L. P., A. J. Coster, J. L. Chau, and C. E. Valladares (2010b), Impact of sudden stratospheric warmings on equatorial ionization anomaly, *J. Geophys. Res.*, *115*, A00G07, doi:10.1029/2010JA015400.

Goncharenko, L. P., A. J. Coster, R. A. Plumb, and D. I. V. Domeisen (2012), The potential role of stratospheric ozone in the stratosphere-ionosphere coupling during stratospheric warmings, *Geophys. Res. Lett.*, *39*, L08101, doi:10.1029/2012GL051261.

Gupta, J. (1973), Movement of the Sq foci in 1958, *Pure Appl. Geophys.*, *110*, 2076–2084.

Hagan, M. E., and J. M. Forbes (2002), Migrating and nonmigrating diurnal tides in the middle and upper atmosphere excited by tropospheric latent heat release, *J. Geophys. Res.*, *107*(D24), 4754, doi:10.1029/2001JD001236.

Hagan, M. E., and J. M. Forbes (2003), Migrating and nonmigrating semidiurnal tides in the upper atmosphere excited by tropospheric latent heat release, *J. Geophys. Res.*, *108*(A2), 1062, doi:10.1029/2002JA009466.

Kalnay, E., M. Kanamitsu, R. Kistler, and W. Cillins (1996), The NCEP/NCAR 40-year reanalysis project, *Bull. Am. Meteorol. Soc.*, *77*, 437–471.

Kerridge, D. (2001), INTERMAGNET: Worldwide near-real-time geomagnetic observatory data, paper presented at Space Weather Workshop: Looking Towards a European Space Weather, Eur. Space Res. and Technol. Cent., Noordwijk, Netherlands.

Le Sager, P., and T. S. Huang (2002), Ionospheric currents and field-aligned currents generated by dynamo action in an asymmetric Earth magnetic field, *J. Geophys. Res.*, *107*(A2), 1025, doi:10.1029/2001JA000211.

Lima, L. M., E. O. Alves, P. P. Batista, B. R. Clemesha, A. F. Medeiros, and R. A. Buriti (2012), Sudden stratospheric warming effects on the mesospheric tides and 2-day wave dynamics at 7°S, *J. Atmos. Sol. Terr. Phys.*, *78–79*, 99–107.

Lindzen, R. S. and S. Chapman (1969), Atmospheric tides, *Space Sci.Rev.*, *10*, 3–188.

Liu, H.-L., and R. G. Roble (2002), A study of a self-generated stratospheric sudden warming and its mesospheric–lower thermospheric impacts using the coupled TIME-GCM/CCM3, *J. Geophys. Res.*, *107*(D23), 4695, doi:10.1029/2001JD001533.

Liu, H.-L., W. Wang, A. D. Richmond, and R. G. Roble (2010), Ionospheric variability due to planetary waves and tides for solar minimum conditions, *J. Geophys. Res.*, *115*, A00G01, doi:10.1029/2009JA015188.

Liu, H., M. Yamamoto, S. Tulasi Ram, T. Tsugawa, Y. Otsuka, C. Stolle, E. Doornbos, K. Yumoto, and T. Nagatsuma (2011), Equatorial electrodynamics and neutral background in the Asian sector during the 2009 stratospheric sudden warming, *J. Geophys. Res.*, *116*, A08308, doi:10.1029/2011JA016607.

Love, J. J. (2008), Magnetic monitoring of Earth and space, *Phys. Today*, *61*, 31–37.

Manney, G. L., et al. (2008), The evolution of the stratopause during the 2006 major warming: Satellite data and assimilated meteorological analyses, *J. Geophys. Res.*, *113*, D11115, doi:10.1029/2007JD009097.

Manney, G. L., M. J. Schwartz, K. Krüger, M. L. Santee, S. Pawson, J. N. Lee, W. H. Daffer, R. A. Fuller, and N. J. Livesey (2009), Aura Microwave Limb Sounder observations of dynamics and transport during the record-breaking 2009 Arctic stratospheric major warming, *Geophys. Res. Lett.*, *36*, L12815, doi:10.1029/2009GL038586.

Matsushita, S., and W.-Y. Xu (1984), Seasonal variations of L equivalent current systems, *J. Geophys. Res.*, *89*(A1), 285–294, doi:10.1029/JA089iA01p00285.

McLandress, C. (2002), The seasonal variation of the propagating diurnal tide in the mesosphere and lower thermosphere. Part II: The role of tidal heating and zonal mean winds, *J. Atmos. Sci.*, *59*, 907–922.

Park, J., H. Lühr, M. Kunze, B. G. Fejer, and K. W. Min (2012), Effect of sudden stratospheric warming on lunar tidal modulation of the equatorial electrojet, *J. Geophys. Res.*, *117*, A03306, doi:10.1029/2011JA017351.

Pedatella, N. M., and J. M. Forbes (2010), Evidence for stratosphere sudden warming-ionosphere coupling due to vertically propagating tides, *Geophys. Res. Lett.*, *37*, L11104, doi:10.1029/2010GL043560.

Pedatella, N. M., J. M. Forbes, and A. D. Richmond (2011), Seasonal and longitudinal variations of the solar quiet (*Sq*) current system during solar minimum determined by CHAMP satellite magnetic field observations, *J. Geophys. Res.*, *116*, A04317, doi:10.1029/2010JA016289.

Pedatella, N. M., H.-L. Liu, A. D. Richmond, A. Maute, and T.-W. Fang (2012), Simulations of solar and lunar tidal variability in the mesosphere and lower thermosphere during sudden stratosphere warmings and their influence on the low-latitude ionosphere, *J. Geophys. Res.*, *117*, A08326, doi:10.1029/2012JA017858.

Richmond, A. D. (1979), Ionospheric wind dynamo theory: A review, *J. Geomagn. Geoelectr.*, *31*, 287–310.

Richmond, A. D. (1989), Modeling the ionosphere wind dynamo: A review, *Pure Appl. Geophys.*, *47*, 413–435.

Richmond, A. D. (1995), Ionospheric electrodynamics using magnetic apex coordinates, *J. Geomagn. Geoelectr.*, *47*, 191–212.

Richmond, A. D., and R. G. Roble (1987), Electrodynamic effects of the thermospheric winds from the NCAR thermospheric general circulation model, *J. Geophys. Res.*, *92*(A11), 12,365–12,376.

Richmond, A. D., E. C. Ridley, and R. G. Roble (1992), A thermosphere/ionosphere general circulation model with coupled electrodynamics, *Geophys. Res. Lett.*, *19*(6), 601–604, doi:10.1029/92GL00401.

Schieldge, J. P., S. V. Venkateswaran, and A. D. Richmond (1973), The ionospheric dynamo and equatorial magnetic variations, *J. Atmos. Terr. Phys.*, *35*, 1045–1061.

Shinbori, A., et al. (2010), Anomalous occurrence features of the preliminary impulse of geomagnetic sudden commencement in the South Atlantic Anomaly region, *J. Geophys. Res.*, *115*, A08309, doi:10.1029/2009JA015035.

Sridharan, S., S. Sathishkumar, and S. Gurubaran (2009), Variabilities of mesospheric tides and equatorial electrojet strength during major stratospheric warming events, *Ann. Geophys.*, *27*, 4125–4130, doi:10.5194/angeo-27-4125-2009.

Sridharan, S., S. Sathishkumar, and S. Gurubaran (2012), Variabilities of mesospheric tides during sudden stratospheric warming events of 2006 and 2009 and their relationship with ozone and water vapour, *J. Atmos. Sol. Terr. Phys.*, *78–79*, 108–115.

Stening, R. J. (2011), Lunar tide in the equatorial electrojet in relation to stratospheric warmings, *J. Geophys. Res.*, *116*, A12315, doi:10.1029/2011JA017047.

Stening, R. J., J. M. Forbes, M. E. Hagan, and A. D. Richmond (1997), Experiments with a lunar atmospheric tidal model, *J. Geophys. Res.*, *102*(D12), 13,465–13,471, doi:10.1029/97JD00778.

Takeda, M. (1990), Geomagnetic field variation and the equivalent current system generated by an ionospheric dynamo at the solstice, *J. Atmos. Terr. Phys.*, *52*, 59–67.

Takeda, M., and H. Maeda (1980), Three-dimensional structure of ionospheric currents: 1. Currents caused by diurnal tidal winds, *J. Geophys. Res.*, *85*(A12), 6895–6899, doi:10.1029/JA085iA12p06895.

Takeda, M., T. Iyemori, and A. Saito (2003), Relationship between electric field and currents in the ionosphere and the geomagnetic Sq field, *J. Geophys. Res.*, *108*(A5), 1183, doi:10.1029/2002JA009659.

Tanaka, Y.-M., Y. Tomikawa, M. K. Ejiri, Y. Yamazaki, K. Yumoto, T. Nagatsuma, and A. Yoshida (2009), Variation in the ionospheric E-region dynamo associated with stratospheric sudden warming in 2009, paper presented at 2009 Autumn Meeting, Meteorol. Soc. of Jpn., Fukuoka, Japan.

Tarpley, J. D. (1970), The ionospheric wind dynamo—I: Lunar tide, *Planet. Space Sci.*, *18*, 1075–1090, doi:10.1016/0032-0633(70)90109-1.

Teitelbaum, H., and C. Cot (1979), Antisymmetric tidal modes under equinoctial conditions induced by ozone heating, *J. Atmos. Terr. Phys.*, *41*, 33–41.

Vineeth, C., T. Kumar Pant, and R. Sridharan (2009), Equatorial counter electrojets and polar stratospheric sudden warmings: A classical example of high latitude-low latitude coupling?, *Ann. Geophys.*, *27*, 3147–3153.

Wang, H., T. J. Fuller-Rowell, R. A. Akmaev, M. Hu, D. T. Kleist, and M. D. Iredell (2011), First simulations with a whole atmosphere data assimilation and forecast system: The January 2009 major sudden stratospheric warming, *J. Geophys. Res.*, *116*, A12321, doi:10.1029/2011JA017081.

Wu, Q., D. A. Ortland, S. C. Solomon, W. R. Skinner, and R. J. Niciejewski (2011), Global distribution, seasonal, and inter-annual variations of mesospheric semidiurnal tide observed by TIMED TIDI, *J. Atmos. Sol. Terr. Phys.*, *73*, 2482–2502.

Yamazaki, Y., et al. (2011), An empirical model of the quiet daily geomagnetic field variation, *J. Geophys. Res.*, *116*, A10312, doi:10.1029/2011JA016487.

Yamazaki, Y., A. D. Richmond, and K. Yumoto (2012a), Stratospheric warmings and the geomagnetic lunar tide: 1958–2007, *J. Geophys. Res.*, *117*, A04301, doi:10.1029/2012JA017514.

Yamazaki, Y., K. Yumoto, D. McNamara, T. Hirooka, T. Uozumi, K. Kitamura, S. Abe, and A. Ikeda (2012b), Ionospheric current system during sudden stratospheric warming events, *J. Geophys. Res.*, *117*, A03334, doi:10.1029/2011JA017453.

Yue, X., W. S. Schreiner, J. Lei, C. Rocken, D. C. Hunt, Y.-H. Kuo, and W. Wan (2010), Global ionospheric response observed by COSMIC satellites during the January 2009 stratospheric sudden warming event, *J. Geophys. Res.*, *115*, A00G09, doi:10.1029/2010JA015466.